International Journal for Housing Science and Its Applications

Publish September 9, 2025. Volume 47, Issue 1 Pages 323-336

https://doi.org/10.70517/ijhsa47126

Research on the optimization design of dynamic characteristics of planetary gear transmission systems based on finite element analysis

Dayu Zhang[1,*]

[1] College of Intelligent Manufacturing, Lishui Vocational and Technical College, Lishui, Zhejiang, 323000, China

Corresponding authors: (e-mail: zhangdayu322@163.com).

Abstract A finite element model of the planetary gear transmission system and a parameter model of the planetary gear train were established, and finite element analysis modeling research on the planetary gear transmission system was conducted. Based on this, genetic algorithms were used to optimize the parameters of the transmission system, and simulation studies on the elastic behavior of the optimized transmission system were conducted under specific operating conditions to verify the rationality of the optimized system's dynamic characteristics. The optimized planetary carrier pin hole node displacement is only 0.312 mm, resulting in minimal positional error. The maximum stress value of the third-stage planetary gear system after optimization is reduced by 0.45 MPa compared to before optimization, while the maximum strain value increases by 0.00058 mm/mm. The input angular velocity, planetary gear angular velocity, and output angular velocity of the optimized system can reach a steady state within the set time, with minimal deviation from theoretical values. The average simulated values of the meshing forces between the sun gear and planetary gears, and between the planetary gears and inner gear ring, are 2916 N and 1275 N, respectively, both close to the theoretical values. This study has preliminarily established an understanding of the transmission characteristics of planetary gear systems, providing a basis for optimizing the design of transmission mechanisms and power configuration in the main spindle drive units of CNC machine tools.

Index Terms finite element analysis, genetic algorithm, dynamic characteristic optimization, planetary gear, transmission system

I. Introduction

A planetary gear transmission system is a mechanical transmission system composed of multiple pairs of gear pairs, shafts, bearings, and housing components. As a complex mechanical structure for transmitting motion and power, the planetary gear transmission system offers advantages such as compact size, lightweight design, high load-carrying capacity, compact structure, high transmission efficiency, wide transmission range, and smooth operation. It is widely applied in fields such as aerospace, automotive, wind power generation, instrumentation, lifting machinery, petrochemical machinery, robotics, and mining machinery [1]-[5]. With the introduction of "Made in China 2025," higher requirements have been placed on the performance of planetary gear transmission systems and their use under various extreme conditions, including the need for new high-performance transmissions that are highly precise, reliable, stable, sensitive, capable of high load capacity, compact in size, lightweight, low in noise, low in vibration, low in friction, low in wear, and energy-efficient [6]-[9]. The theoretical basis and methods for the optimized design of planetary gear transmission systems have become a key area of research.

Due to the large number of gears in planetary gear transmission systems, gear transmission processes generate significant noise and vibration, which may cause malfunctions or damage in certain system components, or even lead to the destruction or failure of the gear system itself [10]-[12]. Additionally, factors such as time-varying meshing stiffness during dynamic meshing, static transmission errors, tooth side clearance, support stiffness, and lubrication friction cause gears to undergo periodic contact-disengagement-contact cycles and strong nonlinear vibrations. These are the primary factors affecting the dynamic performance of gear transmission systems [13]-[16]. Under special conditions, the system may also exhibit amplitude jumps, bifurcation, and chaotic phenomena within certain parameter ranges, severely affecting the stability of the transmission system. The dynamic meshing force under unstable conditions is the primary cause of fatigue fracture, damage, and failure of mechanical system components [17]-[20]. Wang et al. [21] analyzed that in an electromechanical planetary gear transmission system, when the temperature increase range is below 70 °C and the motor speed exceeds 900 rpm, the system exhibits chaotic motion and enters a chaotic state, respectively. Under fluctuations in time-varying meshing stiffness, meshing damping ratio, and transmission error, the system exhibits bifurcation characteristics. Therefore, conducting a dynamic performance analysis of planetary gear transmission systems, studying the influence of various factors on the system's dynamic characteristics, and

achieving advance estimation of system performance provide a theoretical foundation for the dynamic optimization design of transmission systems, enhance design reliability, and hold significant implications for promoting the development of transmission machinery across various industries.

The finite element analysis method is a commonly used engineering analysis method, which not only has high computational accuracy but also adapts to various complex shapes, making it an effective engineering analysis tool for studying structural stress, deformation, and vibration issues [22]-[24]. Its basic principle involves dividing complex structures into finite elements, solving for displacements and stresses within each element, and ultimately determining the behavior of the entire structure. The finite element analysis method uses mathematical approximation techniques to accurately simulate and analyze the dynamic response of actual structures, leading many researchers to apply it to the study of planetary gear transmission systems [25]-[27].

In studies on the optimization of the dynamic characteristics of planetary gear transmission systems, scholars have proposed various methods. Zhang et al. [28] utilized a polynomial response surface surrogate model and genetic algorithms to adjust parameters in the planetary gear transmission system, combining ordered weighted averaging and ideal solution similarity ranking techniques for load tooth contact analysis. Under this optimized structure, the vibration and noise of the transmission system were significantly reduced. Xu et al. [29] mentioned that reducing the backlash gap while maintaining the efficiency of a herringbone planetary gear transmission system is effective in reducing vibration and noise caused by double-sided meshing impacts in the system. Zhang et al. [30] conducted microstructural modifications on gear components in planetary gear transmission systems through numerical and laboratory analyses, effectively alleviating vibration and noise during gear transmission processes. Xu et al. [31] confirmed that tooth profile modification in planetary gear transmission systems can effectively improve time-varying meshing stiffness and sudden changes in meshing tooth surface loads, significantly reducing fluctuations in transmission errors.

Jun et al. [32] investigated the quantitative relationship between gear profile modification parameters and transmission error fluctuations in planetary gear transmission systems, aiming to study the reliability and sensitivity of reducing gear transmission error fluctuations, further confirming the mechanism and effectiveness of gear profile modification in reducing transmission error fluctuations. Mo et al. [33] pointed out under the main resonance characteristic analysis based on the multiscale method that the stability of the Lavinio planetary gearset transmission system is improved by increasing damping, stiffness, and the variability of external loads. Dong et al. [34] found that reducing meshing stiffness or increasing meshing resistance can effectively reduce nonlinear vibrations in a nonlinear bending-torsional load-coupled dynamic model of a planetary gear transmission system. Guo et al. [35] designed high-order elliptical and double-arc pitch curves for non-circular planetary gear transmission systems, adjusted the negative correction coefficient of the planetary gears through multi-body dynamics simulation, reduced tooth interference, and achieved better stability with high-order elliptical gears.

Liang et al. [36] designed an interlocking herringbone planetary gear transmission system consisting of a circular arc convex sun gear, a parabolic concave planetary gear, and a circular arc convex internal gear. Under dynamic modeling, the new system effectively suppressed the vibration defects present in traditional involute tooth profiles. Xiang et al. [37] proposed a multi-objective hierarchical optimization strategy for magnetic planetary gears in a hybrid power transmission system, achieved through a multi-objective genetic algorithm and a double-sided permanent magnet (PM) forming method. Tong et al. [38] employed a particle swarm optimization algorithm to construct a random forest surrogate model, reducing the computational cost of the planetary gear transmission system while maintaining high accuracy. They also designed a decomposition-based adaptive multi-objective evolutionary algorithm to optimize the system's transmission efficiency, gear volume, and reliability.

This paper establishes a finite element geometric model of a planetary gear transmission system in ANSYS Workbench and reasonably designs the parameters of each component to observe the integrity of the model topologically. To improve the dynamic characteristics of the transmission system, the genetic algorithm toolbox in the simulation software is used to optimize the design of the planetary gear transmission system. Through iterative solution of the objective function, the optimal parameter combination of the system is obtained. Simulation studies were then conducted on the elastic behavior and transient dynamics of the optimized system. Additionally, by analyzing the angular velocity, time-domain, and frequency-domain characteristics of the planetary gear train, the optimized system's excellent dynamic characteristics were validated.

II. Finite element analysis study of planetary gear transmission systems

II. A. Establishment of three-dimensional and finite element models

II. A. 1) Three-dimensional models

The foundation of finite element analysis is a three-dimensional model that accurately reflects the actual structure. Currently, various three-dimensional modeling software have their own strengths. Among them, UG can achieve seamless integration with various finite element analysis software, so UG was used to establish a three-dimensional model of the planetary gear transmission [39]. To ensure the three-dimensional model as closely as possible replicates the actual product, it typically includes various detailed features such as bolt holes and chamfers. While these features have minimal impact on the primary analysis results, they significantly increase the number and complexity of the mesh divisions required for mesh generation, as

well as the solution time. If all features of the planetary gear system's gears and planetary carrier structure are divided into finite element meshes, this not only increases the complexity and number of mesh divisions but also greatly prolongs the solution time. Therefore, considering both the finite element analysis results and time costs, geometric cleanup of the planetary gear system's detailed features is performed to facilitate mesh generation and efficient analysis. By adjusting the rotation angle of the reference plane, the planetary gears are assembled with the sun gear and inner gear ring. After confirming no interference, the assembly is arrayed around the sun gear axis. The actual geometric model with detailed features and the model ignoring chamfers, protrusions, bolt holes, and internal splines are used for subsequent analysis.

II. A. 2) Finite element model

ANSYS Workbench can automatically detect the contact relationships of planetary gear assemblies and quickly define contact surfaces. Additionally, the software can rapidly and accurately read the geometric models of planetary gears, enabling topological visualization of the models and verification of their integrity [40]. Therefore, it was selected to establish the finite element model of the planetary gear system. This paper employs a multi-region partitioning method for mesh generation, enabling multiple source faces to be meshed against multiple target faces, rather than using the sweep mesh method, which can only mesh a single source face against a single target face. The elastic modulus of the sun gear, planetary gear, and inner gear ring is 2.58×10^{5} MPa, the Poisson's ratio is 0.251, and the density is 7.64×10^{-9} t/mm^3. Update the component element type, i.e., assign material and element properties to each component, and perform mesh partitioning. The quality of the mesh directly affects the accuracy of the finite element calculation results. A sparse mesh can improve solution speed, but its calculation results may not meet the required accuracy. Since the gear teeth of the planetary gear system in this paper have complex shapes, the mesh division of the gear tooth area directly affects the simulation results. Therefore, the associated center, smoothing, transition, and span center angle settings are set to Fine, Low, Slow, and Fine, respectively.

II. B. Parametric modeling of planetary gear systems

II. B. 1) Establishing a parametric model of planetary gears

When establishing a planetary gear system, the first step is to create finite element models of the sun gear and planetary gears. In the polar coordinate system of the sun gear, the planetary gears are uniformly distributed. Since the orientation of the planetary gears remains unchanged during replication, this can lead to gear tooth interference between the planetary gears and the sun gear, as well as between the planetary gears and the inner ring gear. To address these two interfering issues, it is necessary to first study and analyze the basic operating modes and motion patterns of the planetary gear transmission system. The planetary gear transmission system has diverse operating modes. By adjusting the operating mode, different gear ratios can be achieved, thereby flexibly meeting various practical requirements. In the gear system, the geometric relationships between the gears are fixed and unchanging. Therefore, when studying the motion laws of the planetary gears, different reference frames can be used for research. In this planetary gear system, the sun gear and planetary carrier serve as the input and output, while the inner ring remains stationary. The planetary gears rotate around the sun gear. If the planetary carrier is fixed in place, the planetary gear system is considered a two-stage fixed-axis gear system. The two operating modes are illustrated in Figure 1.

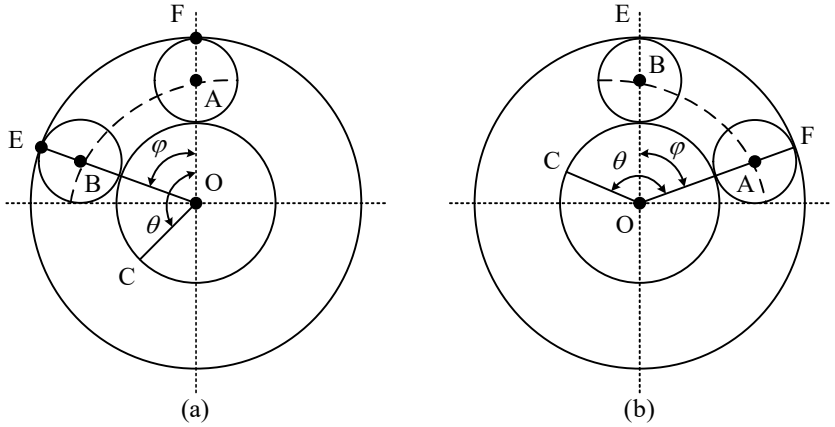

(a) Internal gear ring reference frame (b) Planetary carrier reference frame

Figure 1: Working mode of planetary gear train

If the inner gear ring is taken as the reference frame, then the inner gear ring remains stationary, and when the sun gear and planetary carrier move in and out, the transmission ratio of the planetary gear system is $i_{1H} = 1 + Z_3 / Z_1$. Thus, when the sun gear rotates by $\angle AOC$, the angular displacement of the planetary carrier is $\angle AOB = \angle AOC / i_{1H}$. If the planetary carrier is taken as the reference frame, when the sun gear rotates by $\angle AOC$, $\angle AOB$ corresponds to the angle of rotation of the inner gear ring, and the angle of rotation of the planetary gear ϕ is as follows:

$$\phi = \frac{Z_1}{Z_2} \times \angle AOB \tag{1}$$

Since the planetary gears are evenly distributed around the sun gear, the angle between two adjacent planetary gears and the center of the sun gear is equal, and its size is $360 / k$ (k is the number of planetary gears). From the above equation, it can be seen that in order to achieve uniform distribution and mutual non-interference, the angle of rotation required for the planetary gear to rotate to the adjacent gear position is ϕ as follows:

$$\phi = \frac{Z_1}{Z_2} \times 360 / k \tag{2}$$

After adjusting the rotation angle of the planetary gear, the sun gear and planetary gear mesh, and the teeth of the inner ring gear and planetary gear also mesh, allowing the planetary gears to be evenly distributed throughout the system.

II. B. 2) Establishing contact between gear surfaces

Before establishing a contact pair, it is necessary to identify the areas where contact may occur and define them as target elements and contact elements, which must have the same material properties and be mutually related. This paper uses a command stream approach to establish contact pairs and selects a face-to-face contact method for finite element analysis. The tooth surface of the sun gear is designated as the target surface, with the element type selected as TARGE170. The tooth surface of the planet gear is designated as the contact surface, with the element type selected as CONTA174. During gear meshing transmission, single-tooth meshing or double-tooth meshing may occur, so multiple contact pairs must be defined. Additionally, the contact elements and target elements within the same contact pair must have the same real constants.

II. B. 3) Application of loads and constraints

When performing ANSYS finite element simulation, applying appropriate loads and correctly setting boundary conditions are critical. Selecting different loading methods and setting different boundary conditions can have varying effects on the results of gear contact analysis. This study employs a static analysis method to simulate the meshing state of gears during actual transmission processes. During the simulation, the degrees of freedom of the driven gear shaft bore in all directions and the radial degrees of freedom of the driving gear shaft bore are constrained, and torque is applied to the driving gear. To facilitate the application of loading constraints, the global coordinate system is converted to a cylindrical coordinate system. First, the planetary gear of the driven gear is fixed, and then torque is applied to the sun gear of the driving gear. By constraining the gear center bore node in the radial, axial, and circumferential directions, the loading and constraints are applied. The torque calculation formula is as follows:

$$T = 9.55 \times 10^6 \frac{P}{n} \tag{3}$$

In the formula, T is the torque (N·mm), P is the power, 840 kW, n is the speed of the drive wheel, 1375 r/min.

III. Parameter optimization of planetary gear transmission systems

In order to reduce the size, weight, and complexity of the planetary gear transmission system and analyze the overall energy consumption of the planetary gear, this study used a MATLAB genetic algorithm [41], [42] to optimize the tooth width, module, and number of teeth on the sun gear in the three-stage planetary gear transmission system.

III. A. Genetic Algorithm Computation Process

The operation process of the genetic algorithm is shown in Figure 2.

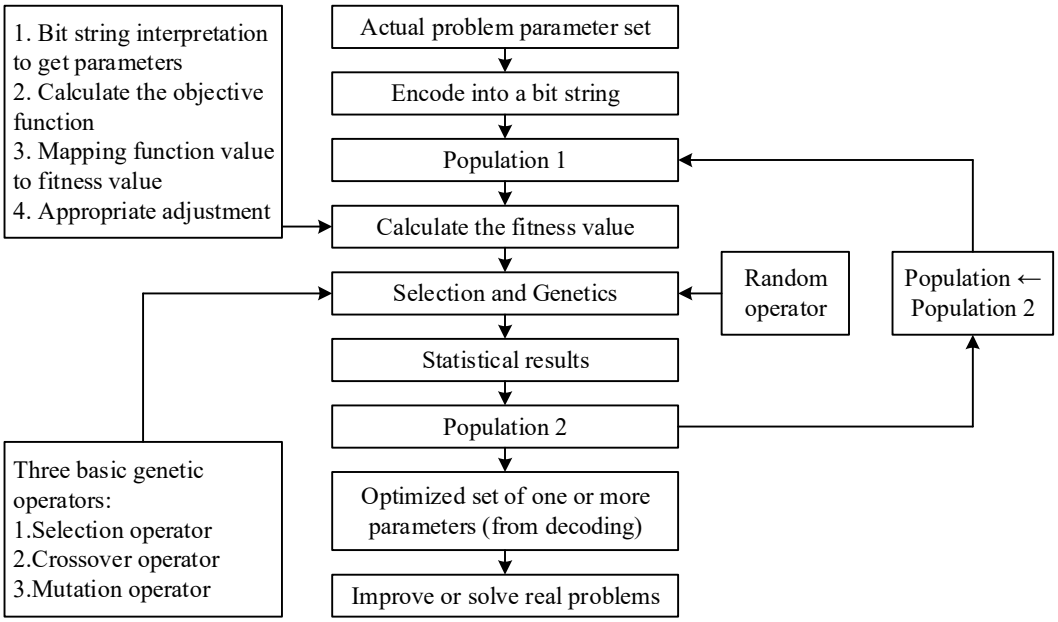

Figure 2: Flowchart of the operation of the genetic algorithm

III. B. Objective Function

In order to make the planetary gear system smaller in volume, lighter in weight, and more compact in structure while maintaining the same load capacity, this paper takes the volume and minimum size of the three-stage planetary gear system as the optimization objectives

A three-stage planetary gear system volume minimization objective function is established, with the sum of the volumes of the sun gear and planetary gears as the objective function:

$$\begin{aligned}&\min F(X)=\frac{\pi}{4}b_1m_1^2[z_{a1}^2+n_{p1}z_{c1}^2]+\frac{\pi}{4}b_2m_2^2[z_{a2}^2+n_{p2}z_{c2}^2]\\&+\frac{\pi}{4}b_3m_3^2[z_{a3}^2+n_{p3}z_{c3}^2]=\frac{\pi}{4}b_1m_1^2z_{a1}^2[1+n_{p1}(\frac{i_{p1}-2}{2})^2]\\&+\frac{\pi}{4}b_2m_2^2z_{a2}^2[1+n_{p2}(\frac{i_{p2}-2}{2})^2]+\frac{\pi}{4}b_3m_3^2z_{a3}^2[1+n_{p3}(\frac{i_{p3}-2}{2})^2]\end{aligned}\tag{4}$$

In the equation, b_i denotes the tooth width of the i th planetary gear train, in mm. m_i denotes the module of the i th planetary gear train, in mm. z_{ai} denotes the number of teeth on the sun gear of the i th planetary gear train. n_{pi} denotes the number of planetary gears in the i th planetary gear train. z_{ci} denotes the number of teeth on the planetary gear in the i th planetary gear train. i_{pi} denotes the gear ratio of the i th planetary gear train.

III. C. Determining Design Variables

From the objective function, it can be seen that the design variables for each stage of the planetary gear system are tooth width, module, number of teeth on the sun gear, and number of planetary gears. Since this paper selects the number of planetary gears for each stage of the planetary gear system to be 3, i.e.:

$n_{p1}=n_{p2}=n_{p3}=3$, the design variables for each planetary gear system are reduced to 3, resulting in a total of 9 design variables for the three-stage planetary gear system. The design variables are:

$$X=[x_1,x_2,x_3,x_4,x_5,x_6,x_7,x_8,x_9]^T=[b_1,m_1,z_{a1},b_2,m_2,z_{a2},b_3,m_3,z_{a3}]^T\tag{5}$$

III. D. Determining Constraints

(1) No root cutting occurs on the pinion:

$$17-z_{a1}\le 017-z_{a2}\le 017-z_{a3}\le 0\tag{6}$$

Since the characteristic parameters of the tertiary planetary gear system are all greater than 3, the minimum number of teeth for each gear should be greater than 17

(2) Minimum tooth width condition:

$$\begin{aligned} 10-b_1 \le 0 \\ 10-b_2 \le 0 \\ 10-b_3 \le 0 \end{aligned} \tag{7}$$

(3) Minimum modulus condition:

$$\begin{aligned} 2-m_1 \le 0 \\ 2-m_2 \le 0 \\ 2-m_3 \le 0 \end{aligned} \tag{8}$$

(4) Relationship between module and tooth width:

$$\begin{aligned} 5m_1-b_1 \le 0 \\ b_1-17m_1 \le 0 \\ 5m_2-b_2 \le 0 \\ b_2-17m_2 \le 0 \\ 5m_3-b_3 \le 0 \\ b_3-17m_3 \le 0 \end{aligned} \tag{9}$$

(5) Gear strength constraints:

Calculation of tooth surface contact stress, such as:

$$\begin{aligned} \sigma_H &= Z_H Z_E Z_c Z_\beta \sqrt{K_A K_U K_H K_{H\alpha} K_{HP} \frac{F_l}{db} \times \frac{u \pm 1}{u}} \le \sigma_{HP} \\ &= \frac{\sigma_{H\lim}}{S_{H\min}} Z_{NT} Z_L Z_V Z_R Z_W Z_X \end{aligned} \tag{10}$$

When calculating the strength of planetary gear transmissions, because internal gear strength is greater than external gear strength under the same material and heat treatment conditions, it is generally necessary to calculate the tooth surface contact strength and root bending strength between the sun gear and planetary gears.

In the equation, σ_H is the tooth surface contact stress. Z_H is the node region coefficient. Z_E is the elasticity coefficient, $\sqrt{N/mm^2}$. Z_ε is the overlap coefficient. Z_β is the helix angle coefficient, which is 1 for straight gears. K_A is the service factor. K_U is the dynamic load factor. K_H is the tooth direction load distribution coefficient. $K_{H\alpha}$ is the load distribution coefficient. K_{HP} is the load unevenness coefficient. F_t is the tangential force on the pitch circle, N. d is the diameter of the pitch circle of the smaller gear, mm. b is the working tooth width, mm. u is the gear ratio. σ_{HP} is the allowable contact stress. $\sigma_{H\lim}$ is the contact fatigue strength, N/mm². $S_{H\min}$ is the minimum safety factor. Z_{NT} is the life coefficient. Z_L is the lubricant coefficient. Z_V is the speed coefficient. Z_R is the roughness coefficient. Z_W is the work hardening coefficient. Z_X is the dimensional coefficient.

Tooth root stress calculation:

$$\begin{aligned} \sigma_F &= Y_{Fa} Y_{Sa} Y_\varepsilon Y_\beta \frac{F_t}{bm_n} K_A K_V K_{F\beta} K_{F\alpha} K_{FP} \le \sigma_{FP} \\ &= \frac{\sigma_{F\lim} Y_{ST} Y_{NT}}{S_{F\min}} Y_{\delta reliT} Y_{RrelT} Y_X \end{aligned} \tag{11}$$

In the equation, σ_F is the root stress. Y_{Fa} is the tooth profile coefficient. Y_{Sa} is the stress correction coefficient. Y_ε is the overlap coefficient. Y_β is the helix angle coefficient. F_i is the tangential force on the pitch circle, N. b is the working tooth width, mm. m_n is the module. K_A is the service factor. K_V is the dynamic load factor. $K_{F\beta}$ is the load distribution factor. $K_{F\alpha}$ is the load allocation factor. K_{FP} is the planetary gear load distribution unevenness coefficient. σ_{FP} is the allowable root stress. $\sigma_{F\lim}$ is the root bending fatigue limit, N/mm². Y_{ST} is the stress correction coefficient. Y_{NT} is the life

coefficient. $S_{F\min}$ is the minimum safety factor. $Y_{\delta reltT}$ is the relative tooth root radius sensitivity coefficient. Y_{RrelT} is the tooth root surface condition coefficient. Y_x is the dimensional coefficient for calculating bending strength.

(6) Transmission ratio error constraint:

$$\frac{|i_p - i|}{i_p} - \varepsilon \le 0 \tag{12}$$

In the formula, i_p is the given transmission ratio. i is the actual transmission ratio. ε is the transmission ratio error.

(7) Adjacency condition:

$$d_{ac} < 2a'_{ac} \sin\frac{\pi}{n_p} \tag{13}$$

In the formula, d_{ac} is the diameter of the tip circle of the planetary gear. a'_{ac} is the center distance of the meshing pair of gears a and c. n_p is the number of planetary gears.

IV. Simulation study on optimization of system parameters and optimization characteristics

IV. A. Elastic behavior

The finite element models in the system are condensed to extract the corresponding mass and stiffness matrices, and this calculation process can be performed in general finite element software. At the same time, deformation smoothness is used as an evaluation index, and the performance of each stiffness matrix is verified by means of the load transfer behavior between the condensed nodes. Finally, load boundary conditions are applied to the system model, and a global quasi-static elastic mechanical behavior analysis is performed to obtain the node displacement responses of each elastic component under rated operating conditions. In the system-level simulation analysis, the planetary gear sequentially transmits the power received from the sun gear to the double-row tapered roller bearings (DRTRB) and the planetary pin shaft, ultimately applying the load to the planetary carrier pin holes. Figure 3 shows the calculated results of the elastic deformation of the planetary carrier and the load distribution on each DRTRB. As shown in the figure, under system rated operating conditions, the node displacement at the planetary carrier pin holes is only 0.312 mm, which does not exceed 1 mm. This indicates that the planetary shaft of the transmission system may exhibit positional errors after parameter optimization, but the error magnitude is small and will not affect the root stress response results in the planetary gear system.

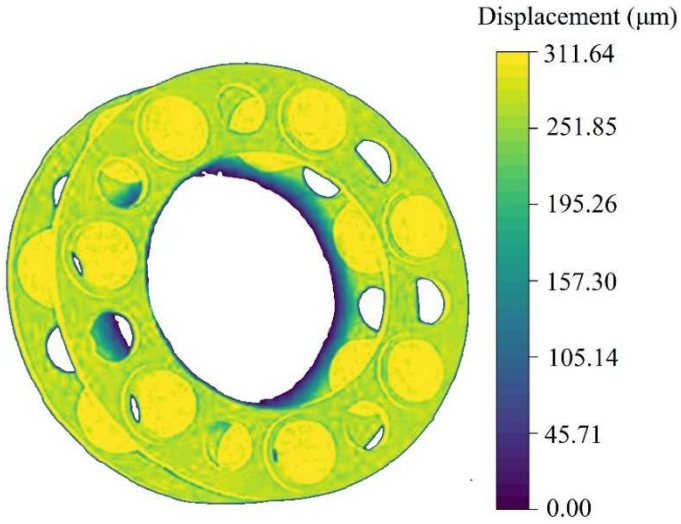

Figure 3: Planetary displacement cloud

In system-level simulation analysis, it is necessary to obtain the rim displacement response of the planetary gear and the node displacement response of the gear teeth to provide the required displacement boundary conditions for the secondary submodel of root stress calculation. Figure 4 shows the calculation results of elastic deformation and stress distribution of the planetary gear under rated operating conditions. The structural integrity of the system model ensures that the results simultaneously consider the effects of elastic deformation of the planetary carrier and planetary shaft, bearing clearance, and

other factors. The comparison between the original contour of the planetary gear and its loaded deformation contour (with deformation scaled up) is shown in Figure 4(a). It can be observed that the rim of the planetary gear is approximately circular and does not exhibit significant elastic deformation. Figure 4(b) shows the stress distribution contour map of the planetary gear under load. The figure identifies the two gear teeth that mesh with the sun gear and inner gear ring. The high-stress zones are located at the root of these two gear teeth on the loaded side, with the maximum root stress value reaching 306.76 MPa. From the figure, it can also be observed that the root stress values of the teeth not currently engaged are close to zero, primarily due to the lack of significant elliptical deformation in the rim structure.

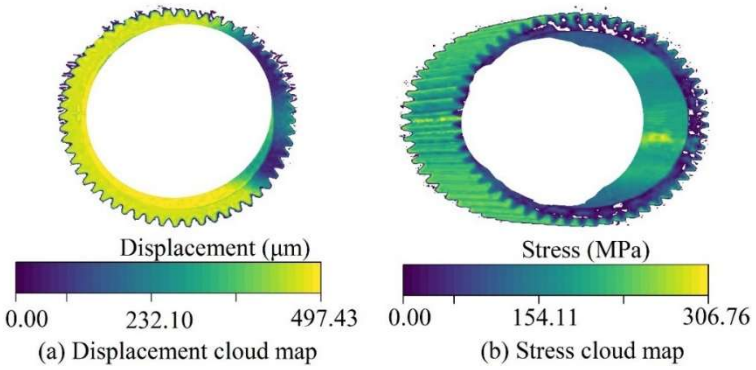

Figure 4: Planetary gear analysis results

In system-level simulation analysis, the node displacement responses of the sun gear's rim and teeth are reflected in the displacement contour plot of the input shaft, with the elastic deformation results shown in Figure 5. As can be seen from the figure, the sun gear and inner gear ring exhibit the same deformation trend, with elastic deformation zones present near the teeth in contact with the planetary gears. The flexible design of the sun gear's rim structure ensures that each high deformation zone is uniformly covered by multiple teeth in the circumferential direction. The thin-walled rim and cantilever support conditions of the inner gear ring cause each high deformation zone to shift equally in the axial direction. These elastic behavior characteristics will significantly influence the root stress distribution and stress levels of the corresponding gears.

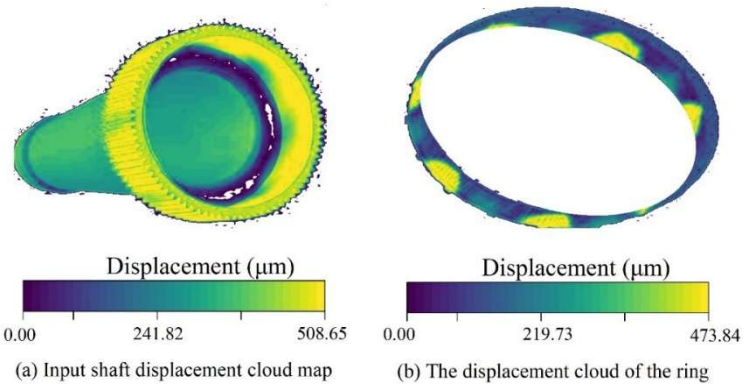

Figure 5: Elastic deformation result

IV. B. Transient Dynamics

For the third-stage planetary gear reducer, the mesh is refined for the critical tooth contact surfaces. For the sun gear-planetary gear pair, the sun gear's entire tooth surface is designated as the target surface, while the planetary gear's tooth surface serves as the contact surface. For the planetary gear-ring gear pair, the planetary gear's tooth surface is designated as the target surface, and the ring gear's tooth surface serves as the contact surface. The ring gear is fixed to the base, while the sun gear and planetary carrier rotate around the base, with the planetary gear shaft serving as the reference plane for orbital motion. Set the planetary gears and planetary gear carrier planetary gear shafts as body-to-body contacts to enable the planetary gears' rotation and revolution. Apply a torque load of 42.15 kN·m to the third-stage planetary gear carrier of the transmission system, set the sun gear to rotate by 60°, select iterative sub-steps to improve computational accuracy, and perform transient dynamic simulation analysis. To improve computational accuracy, the mesh size is reduced for the contact surfaces and gear tooth transition areas of the planetary gear system, and mesh refinement is performed using tetrahedral meshes. To improve

computational speed, larger mesh sizes than those for gear contact surfaces are used for other non-gear contact surfaces, with the mesh size set to 4×10^{-3} m, resulting in 507,329 mesh elements after division.

Based on the simulation results, the stress-strain and total deformation contour plots of the planetary gear system before and after parameter optimization for the third stage of the transmission system are shown in Figures 6 and 7, respectively. Based on the data analysis of the two figures, the maximum stress values before and after parameter optimization of the third-stage planetary gear system are 7.58 MPa and 7.13 MPa, respectively, and the maximum strain values are 0.00415 mm/mm and 0.00473 mm/mm, respectively. The maximum stress and strain occur at the contact surface between the sun gear and the planetary gears. The maximum stress and strain in the external meshing pair are greater than those in the internal meshing pair. The simulation results are consistent with the principles of gear meshing and the motion characteristics of the planetary gear system, thereby validating the accuracy of the model. After parameter optimization of the gears, the stress on the sun gear teeth is reduced because the optimized sun gear-planetary gear tooth surface contact line is longer, resulting in reduced stress on the teeth. The gears are less prone to failure compared to before, and reliability is enhanced

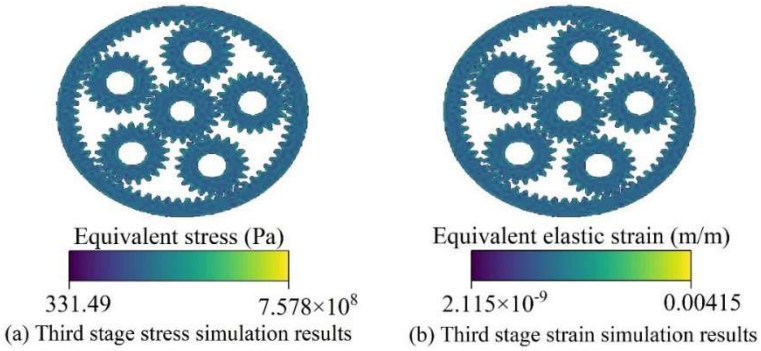

(a) Third stage stress simulation results (b) Third stage strain simulation results

Figure 6: Optimization of the simulation results of the former transient dynamics

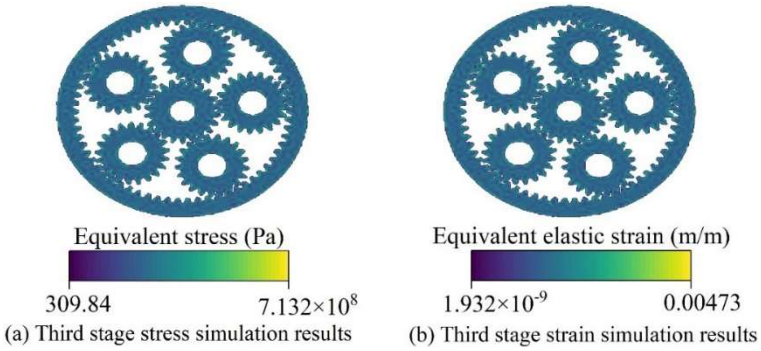

(a) Third stage stress simulation results (b) Third stage strain simulation results

Figure 7: Optimal post-transient dynamic simulation results

IV. C. Dynamic Characteristics

Compared with traditional gear transmission systems, the optimized planetary gear system described in this paper features fast response speed, high transmission efficiency, large transmission torque, high performance, wide speed regulation range, high positioning accuracy, and compact structure. The circumferentially distributed planetary gears not only share the load but also offset the radial force acting on the center gear. This section will conduct a dynamic characteristic study of the optimized planetary gear system to provide a basis for optimizing the design of transmission mechanisms and power configuration in the main spindle drive system of CNC machine tools.

IV. C. 1) Kinematic analysis

The input speed of the planetary gear system is set to 2000 r/min, i.e., 12000 deg/sec, and the output speed is set to 500 r/min, i.e., 3000 deg/sec. The speed of the planetary gear is:

$$\frac{n_1 - n_3}{n_c - n_3} = -\frac{z_c}{z_a} \tag{14}$$

In the formula, n_1 is the rotational speed of the sun gear, n_3 is the rotational speed of the planetary carrier, n_c is the rotational speed of the planetary gear

Substituting the above data into the above equation yields n_c = 1000 r/min, or 6000 deg/sec. Add a selected drive to the rotating joint with a magnitude of 12000 deg/sec, set the start time to 6 s, the simulation time to 15 s, the step size to 0.1, and the number of steps to 600. After running the solution, the input angular velocity, planetary gear angular velocity, and output angular velocity curves of the planetary gear transmission system are shown in Figure 8. As can be seen from the figure, the obtained input angular velocity curve aligns with the drive settings, i.e., it starts within 6 seconds, and at the 6-second mark, the input angular velocity, planetary gear angular velocity, and output angular velocity reach 12,000, 6,000, and 3,000 deg/sec, respectively, and remain constant for the subsequent 9 seconds. The trend of angular velocity changes aligns with the simulation settings.

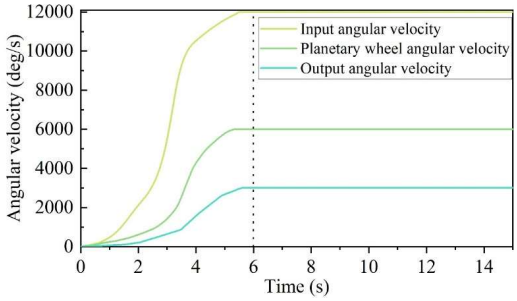

Figure 8: The curve of the Angle velocity of the transmission system

As shown in the figure above, the input angular velocity is significantly greater than the output angular velocity, indicating that the system conforms to the speed reduction characteristics of a transmission system. The simulated transmission ratio is calculated to be 3.999, which differs from the theoretical transmission ratio of 4 by only 0.025%, demonstrating that the established simulation model is accurate and reliable. A comparison of the simulation values with the theoretical values yields the results shown in Table 1. As shown in the table, the angular velocity error of the planetary gear is only 0.01262%, and the angular velocity error of the output shaft is only 0.017%, further validating the correctness of the parameter optimization model for the planetary gear transmission system proposed in this paper.

Table 1: Angular velocity comparison

Project	Input angular velocity	Planetary wheel angular velocity	Output angular velocity
Simulation value	12000	6000.757	3000.51
Theoretical value	12000	6000	3000
Error (%)	0	0.01262	0.017

IV. C. 2) Kinetic analysis

This section further conducts a dynamic simulation analysis of the optimized transmission system.

First, the meshing force between the sun gear and the planetary gear is calculated. The force analysis of the straight-toothed cylindrical gear is shown in Figure 9.

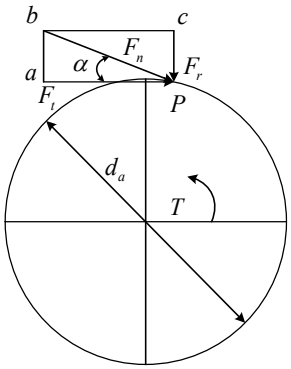

Figure 9: Force Analysis of Spur Cylindrical Gear Teeth

As shown in the figure, the normal load F_n acting on the tooth surface along the meshing line is perpendicular to the tooth surface and is orthogonally decomposed into a circumferential force F_t and a radial force F_r at node P. The force on the sun gear and planetary gear 1 meshing pair is as follows:

$$F_t = \frac{2T_t}{d_a} \tag{15}$$

$$F_r = F_t \tan\alpha \tag{16}$$

$$F_n = \frac{F_1}{\cos\alpha} \tag{17}$$

In the formula, T_1 is the torque transmitted by the sun gear, d_a is the diameter of the pitch circle of the sun gear

Next, calculate the forces acting on the planetary gear 1 and the inner ring gear based on the meshing forces between the planetary gear and the inner ring gear as follows:

$$F_t = \frac{2T_2}{d_c} \tag{18}$$

$$F_r = F_t \tan\alpha \tag{19}$$

$$F_n = \frac{F_t}{\cos\alpha} \tag{20}$$

In the equation, T_2 is the torque transmitted by the planetary gear, d_c is the pitch diameter of the planetary gear.

Based on the transmission principle of the planetary gear system, the motion and power transmission of the gear system are achieved through gear meshing. Therefore, the contact method is used for the dynamic analysis of the transmission system. To improve simulation efficiency and reduce simulation time, the simulation time is set to 1 s. A rotational drive with a speed of 12,000 deg/sec is added to the sun gear rotational pair, and the motor startup time is set to 0.5 s.

(1) Time-domain analysis

The time-domain diagrams of the meshing forces between the sun gear and planetary gears, and between the planetary gears and inner ring gear, obtained from the dynamic simulation analysis are shown in Figures 10 and 11, respectively. As can be seen from the figures, at the instant the servo motor starts, due to a sudden change in speed, internal gear excitation occurs, resulting in impact, and the contact force (meshing force) exhibits significant fluctuations. Once the system enters the stable transmission phase, the meshing force fluctuates around a mean value and exhibits periodic changes, reflecting the characteristic of periodic meshing and disengagement of the gears. The engagement force between the planetary gear and the inner gear ring exhibits relatively smaller fluctuations in amplitude compared to the engagement force between the sun gear and the planetary gear once the speed enters a stable phase. This indicates that the amplitude of engagement force fluctuations decreases as the transmission speed decreases. Occasional noticeable fluctuations are attributed to the static load condition. The average simulated meshing force between the sun gear and planetary gears is 2,916 N, with a theoretical value of 3,000 N. The average simulated meshing force between the planetary gears and inner gear ring is 1,275 N, with a theoretical value of 1,300 N. The theoretical values and simulated results are similar, further validating the reliability of the model.

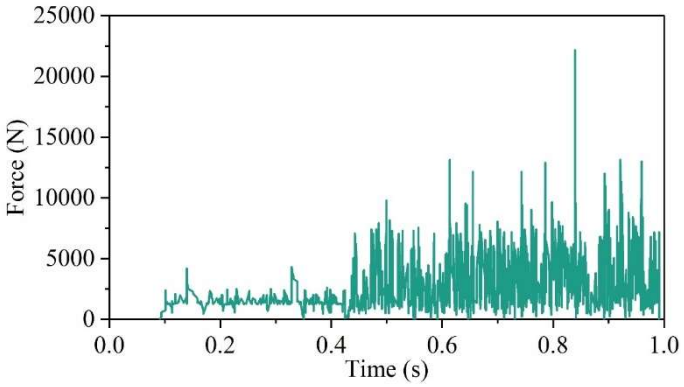

Figure 10: The solar wheel and the planetary wheel meshing force time domain diagram

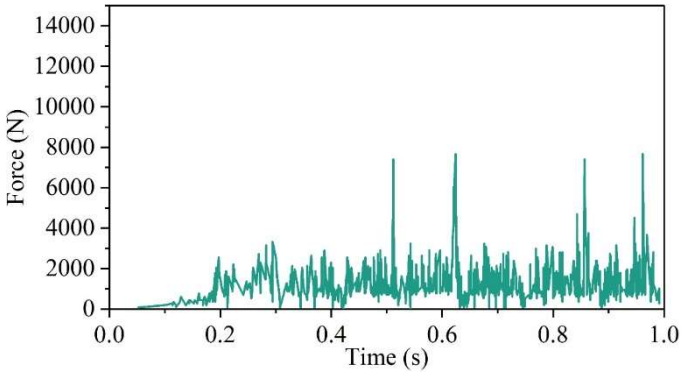

Figure 11: Time domain diagram of planetary wheel and inner tooth coil mesh

(2) Frequency domain analysis

The meshing forces of the gear transmission are subjected to a Fourier transform, yielding the frequency domain diagrams of the meshing forces between the sun gear and the planetary gears, and between the planetary gears and the inner gear ring, as shown in Figures 12 and 13, respectively. As can be seen from the figures, the meshing forces exhibit periodic variations, with a period corresponding to the meshing cycle of a single gear tooth, and the frequency magnitude corresponding to the frequency of the higher-frequency line in the figure. As shown in Figure 12, there are two prominent peaks in the frequency domain diagram. One is at 255.26 Hz, which is the rotational frequency of the sun gear, and the other is at 519.28 Hz, which is the meshing force frequency. These values are close to the theoretical values of 250 Hz and 550 Hz, respectively. As shown in Figure 13, there are also two prominent peaks in the frequency domain diagram. One is at 248.05 Hz, which is the rotational frequency of the planetary gear, and the other is at 557.24 Hz, which is the meshing force frequency. These values are close to the corresponding theoretical values of 250 Hz and 550 Hz. Through the dynamic characteristic analysis in this section, the stability of the planetary gear transmission system after parameter optimization has been proven, further demonstrating the reliability of the virtual prototype

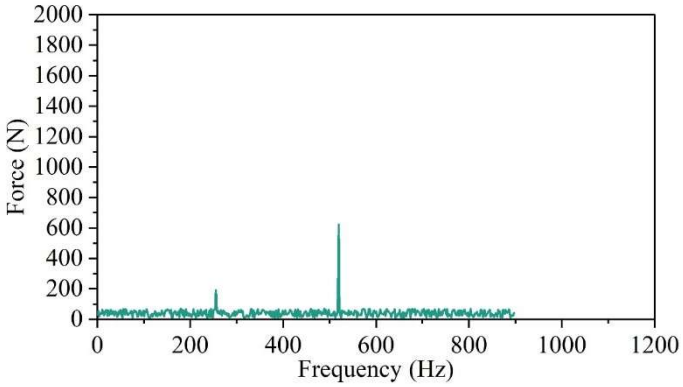

Figure 12: The sun wheel and the planetary wheel mesa force diagram

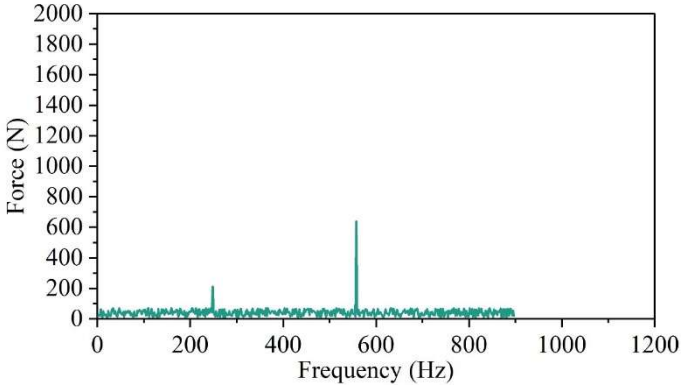

Figure 13: Planetary wheel and inner tooth coil mesh force frequency domain diagram

V. Conclusion

This paper is based on the finite element analysis of planetary gear transmission systems. By establishing a finite element model and parameterizing the planetary gear system, it provides a model foundation for optimizing the dynamic characteristics of the transmission system. The optimization of the transmission system aims to minimize the volume of the three-stage planetary gear transmission system. A genetic algorithm is used to optimize the parameters of the transmission system under constraint conditions. Through simulation analysis of system elastic behavior and transient dynamics, the rationality of the optimized system is verified. Further analysis of the kinematics and dynamics of the transmission system is conducted to gain a deeper understanding of the dynamic characteristics of the optimized transmission system. The following conclusions are drawn from the study:

The optimized transmission system exhibits a smaller tendency for elastic deformation, with the maximum root stress values of the sun gear and inner gear ring reaching 306.76 MPa. After optimization, the stress on the gears decreases from 7.58 MPa to 7.13 MPa, resulting in higher safety compared to the pre-optimization state. The input angular velocity, planetary gear angular velocity, and output angular velocity of the system can reach the rated values within 6 seconds of operation, with an error of less than 0.02%. In the frequency domain analysis, the frequency spectra of the meshing forces between the sun gear and planetary gears, as well as between the planetary gears and inner gear ring, are close to the theoretical values

References

[1] Wei, J., Zhang, A., Shi, L., Qin, D., & Lim, T. C. (2020). Modeling and dynamic characteristics of planetary gear transmission in non-inertial system of aerospace environment. Journal of Mechanical Design, 142(3), 031103.

[2] He, G., Ding, K., Li, W., & Li, Y. (2017). Frequency response model and mechanism for wind turbine planetary gear train vibration analysis. IET Renewable Power Generation, 11(4), 425-432.

[3] Wang, J., Liu, N., Wang, H., & Guo, L. (2021). Nonlinear dynamic characteristics of planetary gear transmission system considering squeeze oil film. Journal of Low Frequency Noise, Vibration and Active Control, 40(2), 823-851.

[4] Wang, X., & Ma, D. (2024, June). Research on dynamic characteristics of mining two-stage planetary gear train considering with eccentricity fault. In Fourth International Conference on Mechanical, Electronics, and Electrical and Automation Control (METMS 2024) (Vol. 13163, pp. 428-434). SPIE.

[5] Zhang, C., Wei, J., Niu, R., Hou, S., & Zhang, S. (2023). Similarity and experimental prediction on load sharing performance of planetary gear transmission system. Mechanism and Machine Theory, 180, 105163.

[6] Liu, C., Yang, C., Zhao, Y., Luo, J., & Chen, X. (2023). Dynamic modeling and analysis of high-speed flexible planetary gear transmission systems. Alexandria Engineering Journal, 80, 444-464.

[7] Xiao, Z., Chen, F., & Zhang, K. (2021). Analysis of dynamic characteristics of the multistage planetary gear transmission system with friction force. Shock and Vibration, 2021(1), 8812640.

[8] Lyu, H., Wang, S., Ma, L., Zhang, X., & Pecht, M. (2022). Reliability modeling for planetary gear transmission system considering dependent failure processes. Quality and Reliability Engineering International, 38(1), 229-247.

[9] Yang, H., Shi, W., Guo, L., Zhao, Y., & Yuan, R. (2022). Study on mesh stiffness and sensitivity analysis of planetary gear system considering the deformation effect of carrier and bearing. Engineering Failure Analysis, 135, 106146.

[10] Zhou, W., Zuo, Y., & Zheng, M. (2018). Analysis and optimization of the vibration and noise of a double planetary gear power coupling mechanism. Shock and Vibration, 2018(1), 9048695.

[11] Chen, X., & Feng, Z. (2017). Time-frequency analysis of torsional vibration signals in resonance region for planetary gearbox fault diagnosis under variable speed conditions. IEEE Access, 5, 21918-21926.

[12] Wang, Y. R., Jin, Q., Sun, G. D., & Sun, C. F. (2019). Planetary gearbox fault feature learning using conditional variational neural networks under noise environment. Knowledge-Based Systems, 163, 438-449.

[13] Chen, R., Zhou, J., & Sun, W. (2018). Dynamic characteristics of a planetary gear system based on contact status of the tooth surface. Journal of Mechanical Science and Technology, 32(1), 69-80.

[14] Dai, H., Chen, F., Xun, C., & Long, X. (2022). Numerical calculation and experimental measurement for gear mesh force of planetary gear transmissions. Mechanical Systems and Signal Processing, 162, 108085.

[15] Hu, S., Fang, Z., Xu, Y., Guan, Y., & Shen, R. (2021). Meshing impact analysis of planetary transmission system considering the influence of multiple errors and its effect on the load sharing and dynamic load factor characteristics of the system. Proceedings of the Institution of Mechanical Engineers, Part K: Journal of Multi-body Dynamics, 235(1), 57-74.

[16] Wang, X., Xiang, C., Li, C., Li, S., Shao, Y., & Wang, L. (2020). Effect of roughness on meshing power loss of planetary gear set considering elasto-hydrodynamic lubrication. Advances in Mechanical Engineering, 12(2), 1687814020908422.

[17] Wang, J., Luo, Z., Shan, Z. A., & Yi, Y. (2024). Chaotic characteristic analysis of planetary gear transmission system under multi-coupling factor considering thermal effect. Journal of Vibration Engineering & Technologies, 12(3), 4287-4311.

[18] Shen, G., Xiang, D., Zhu, K., Jiang, L., Shen, Y., & Li, Y. (2018). Fatigue failure mechanism of planetary gear train for wind turbine gearbox. Engineering Failure Analysis, 87, 96-110.

[19] Wang, X. (2018). Stability research of multistage gear transmission system with crack fault. Journal of Sound and Vibration, 434, 63-77.

[20] Xu, X., Chen, J., Lin, Z., Qiao, Y., Chen, X., Zhang, Y., ... & Li, Y. (2022, February). Optimization design for the planetary gear train of an electric vehicle under uncertainties. In Actuators (Vol. 11, No. 2, p. 49). MDPI.

[21] Wang, J., Bi, X., & Mo, R. (2024). Nonlinear dynamics analysis of electromechanical planetary gear systems with temperature effects considered. Engineering Computations, 41(3), 516-544.

[22] He, S., Tang, T., Xu, E., Ye, M., & Zheng, W. (2020). Vibration control analysis of vehicle steering system based on combination of finite-element analysis and modal testing. Journal of Vibration and Control, 26(1-2), 88-101.

[23] Czakó, A., Řehák, K., Prokop, A., & Ranjan, V. (2020). Determination of static transmission error of helical gears using finite element analysis. Journal of Measurements in Engineering, 8(4), 167-181.

[24] Yuan, W. H., Wang, H. C., Zhang, W., Dai, B. B., Liu, K., & Wang, Y. (2021). Particle finite element method implementation for large deformation analysis using Abaqus. Acta Geotechnica, 16(8), 2449-2462.
[25] Gayen, D., Chakraborty, D., & Tiwari, R. (2017, December). Finite element analysis for dynamic response of rotor-bearing system with cracked functionally graded turbine shaft. In Gas Turbine India Conference (Vol. 58516, p. V002T05A001). American Society of Mechanical Engineers.
[26] Mihailidis, A., Korbetis, G., Drivakos, N., & Nerantzis, I. (2018). Finite element method based analysis of planetary gear systems considering backlash and manufacturing deviations. Power Transmission Engineering, 46-50.
[27] Cooley, C. G., & Hood, A. A. (2023, August). Investigation of Planetary Gear Elastic Vibrations Using a Finite Element/Contact Mechanics Formulation. In International Design Engineering Technical Conferences and Computers and Information in Engineering Conference (Vol. 87400, p. V012T12A024). American Society of Mechanical Engineers.
[28] Zhang, Q., Xu, S., Yuan, Y., Yan, X., Huang, D., Yu, J., ... & Zhan, G. (2023). Multi-objective optimization design and dynamic characteristic analysis based on planetary gear transmission. J. Netw. Intell, 8(3), 639-657.
[29] Xu, X., Ge, H., Wu, H., & Jia, H. (2024). Research on nonlinear characteristics of herringbone planetary gear transmission system considering double-sided meshing impact. Nonlinear Dynamics, 112(5), 3195-3215.
[30] Zhang, J., Guo, H., Yu, H., & Zhang, T. (2020). Numerical and experimental investigation on nonlinear dynamic characteristics of planetary gear train. Journal of Theoretical and Applied Mechanics, 58(4), 1009-1022.
[31] Xu, X., Fan, X., Diao, P., & Liu, H. (2019). An investigation on the influence of modification parameters on transmission characteristics of planetary gear system. Journal of Mechanical Science and Technology, 33(7), 3105-3114.
[32] Jun, Z., Wei-min, T., Qin, C., & Tao, C. (2020). Reliability sensitivity analysis of tooth modification on dynamic transmission error of helical planetary gears. Proceedings of the Institution of Mechanical Engineers, Part C: Journal of Mechanical Engineering Science, 234(19), 3903-3918.
[33] Mo, S., Huang, T., Hu, Y., Liu, Y., Zhou, Y., Zhang, J., & Zhang, W. (2025). Nonlinear Dynamics of Ravigneaux Planetary Gearset in Automobile Transmission Systems. International Journal of Bifurcation and Chaos, 35(05), 2550058.
[34] Dong, H., Bi, Y., Liu, Z. B., & Zhao, X. L. (2021). Establishment and analysis of nonlinear frequency response model of planetary gear transmission system. Mechanical Sciences, 12(2), 1093-1104.
[35] Guo, J., Dong, C., Liu, Y., Li, D., & Wang, J. (2025). Optimization design and stability investigation of non-circular planetary gears transmission system. Flow Measurement and Instrumentation, 104, 102910.
[36] Liang, D., Hu, H., & Wu, Y. (2024). Geometric design and dynamic characteristics analysis of a novel herringbone planetary gear. Proceedings of the Institution of Mechanical Engineers, Part K: Journal of Multi-body Dynamics, 14644193251355123.
[37] Xiang, Z., Zhu, X., Jiang, M., & Quan, L. (2021). Multi-objective-layered optimization of a magnetic planetary gear for hybrid powertrain. IEEE Journal of Emerging and Selected Topics in Power Electronics, 10(1), 934-944.
[38] Tong, S., Yan, X., Yang, L., & Yang, X. (2024). A Novel Multi-Objective Dynamic Reliability Optimization Approach for a Planetary Gear Transmission Mechanism. Axioms, 13(8), 560.
[39] Xiaopeng Chang,Siyu Chen,Xiyu Zhang,Bangcheng Zhang & Bo Yu. (2025). Design of Steering Joint System Based on UG 3D Software and Intelligent Algorithm. Procedia Computer Science,262,378-386.
[40] Daniel Winarski,Kip P. Nygren & Tyson Winarski. (2025). Digital-Twin of the National Collegiate Athletic Association Specified Energy Rebound Testing Device: Kinetic-Energy Absorption by a Basketball Rim and Backboard Modeled with ANSYS Workbench Finite Element Analysis. Vibration,8(1),9-9.
[41] Xiaofei Huang,Junwei Yan,Xuan Zhou,Zhixian Yang & Xiaofeng Huang. (2025). Energy-efficient optimization method for air conditioning terminal systems in IDC based on genetic algorithm. Energy,333,137502-137502.
[42] Mahmoud Karimi & Halis Simsek. (2025). Life cycle assessment and techno-economic optimization of biocrude oil production from microalgae via hydrothermal liquefaction using genetic algorithms. Journal of Cleaner Production,520,146104-146104.